

Simulations of Driven Field Line Resonances in the Earth's Magnetosphere

R. RANKIN, J.C. SAMSON, AND P. FRYCZ

Canadian Network for Space Research, University of Alberta, Edmonton, Alberta, Canada

Using a compressible, three-dimensional resistive magnetohydrodynamic (MHD) computer simulation code, we examine the evolution of standing wave field line resonances (FLRs) in the nightside of the Earth's magnetosphere. The MHD code that is used allows for a full nonlinear description and enables us to follow the evolution of FLRs to large amplitude. We take as our MHD driver a source of fast-mode waves incident from the direction of the magnetopause boundary layer. The ambient density and geomagnetic field are such that the fast mode waves have turning points at radial distances between 8 and 10 R_E in the equatorial plane. The fast-mode angle of incidence is selected such that tunneling of the wave from the turning point to the resonance point leads to resonant mode conversion of energy from compressional waves to shear Alfvén waves. We determine whether kinetic effects or finite electron inertia effects are likely to become important during the nonlinear evolution of the FLRs. For this to occur, the FLRs must narrow to the point where the radial scale size is several ion gyroradii or less or to the point where the equatorial width of the resonance maps to several electron inertia lengths in the polar magnetosphere. It is shown that the resonances do narrow to the point where kinetic effects are likely to be important and that, in contrast to estimates in previously published work indicating that narrowing would take hundreds of wave cycles, this occurs within a few cycles of the driver field, consistent with observations of FLRs in the high-latitude ionosphere.

INTRODUCTION

A fundamental problem associated with magnetohydrodynamic (MHD) wave propagation in the Earth's magnetosphere concerns the possibility of mode conversion of compressional MHD wave energy to shear Alfvén waves and, ultimately, to kinetic Alfvén waves or electron inertia waves in association with field line resonances (FLRs). If mode conversion to kinetic Alfvén waves or electron inertia waves occurs, a variety of processes are possible, including the acceleration of electrons in the parallel fields associated with the FLRs; in particular, the FLRs might play a role in the formation of certain types of auroral arcs [Hasegawa, 1976; Goertz, 1984]. There is now direct evidence that FLRs play an important role in modulating the electron precipitation in auroral arcs [Samson *et al.*, 1991; Xu *et al.*, 1993]. At present, there is no firm evidence that this modulation is due to kinetic Alfvén waves or electron inertia waves, but the possibility of kinetic effects occurring is strong. In order for kinetic effects to become important, the FLR must narrow to a point where its radial scale size is on the order of several ion gyroradii or less. Many high-latitude FLRs are observed on magnetic field lines which map to the plasmasheet, where ion gyroradii are on the order of hundreds of kilometers, and so the resonances must narrow to several hundred kilometers or less in the equatorial plane for ion gyroradius effects to become important. In the equatorial plane, it is unlikely that FLRs will narrow to the point where their radial scale size is comparable to the electron inertial length. However, electron inertia effects will become important provided the equatorial width of the resonance maps to several electron inertia lengths in the polar magnetosphere at altitudes of approximately 1 R_E . In particular, above the auroral ionosphere, electron inertia lengths are of the order of 1 km or so, which maps to roughly 50 km in the equatorial plane, and so conservatively the resonances

must narrow down to a few hundred kilometers in the equatorial plane for electron inertia effects to play a significant role.

Losses due to Joule heating of the ionosphere by the FLR will broaden the resonance and may prevent mode conversion to kinetic Alfvén or electron inertia waves from occurring. Calculations using typical dayside and nightside height-integrated conductivities and based on simple linear theory of FLRs (see below) indicate that in both the dayside and nightside regions the widths of the resonances should stabilize at values comparable to or less than a typical ion gyroradius in the plasmasheet. Satellite measurements of the radial width of FLRs have found widths as small as 0.2 R_E [Hughes *et al.*, 1978; Singer *et al.*, 1982]. In order for kinetic effects to become important in FLRs in the magnetosphere, it is only necessary for this narrowing to occur within a reasonably small number of wave cycles. Experimental observations of 1- to 4-mHz FLRs in the auroral ionosphere suggest that typical wavetrains associated with incident compressional mode energy last for only several cycles [Walker *et al.*, 1992], and so narrowing of the FLR must occur within this time frame. Allan and Poulter [1989] have suggested that it would take on the order of several hundred cycles for FLRs to narrow to the point where kinetic effects become important, thereby effectively ruling out kinetic effects in FLRs in the magnetosphere. Nevertheless, some computer studies [Inhester, 1987] and experimental measurements [Walker *et al.*, 1992] indicate that narrowing occurs much more rapidly than this. Walker *et al.* [1992] found that a FLR measured by HF-radar in the auroral region had narrowed to a latitudinal width of approximately 40 km within one or two wave cycles. In fact, the width may have narrowed even further, but the radar could not resolve features narrower than 40 km. A 40-km width in the ionosphere maps to a radial width of approximately 2000 km in the equatorial plane, which is still rather large for kinetic effects to become important, except for more energetic plasmas. Nevertheless, the experimental measurements still point to the possibility of kinetic effects if further narrowing occurs.

In order to address the problem of the evolution of FLRs to large amplitudes and very short scales, we have performed computer simulations which allow for a three-dimensional configura-

Copyright 1993 by the American Geophysical Union.

Paper number 93JA02083.
0148-0227/93/93JA-02083\$05.00

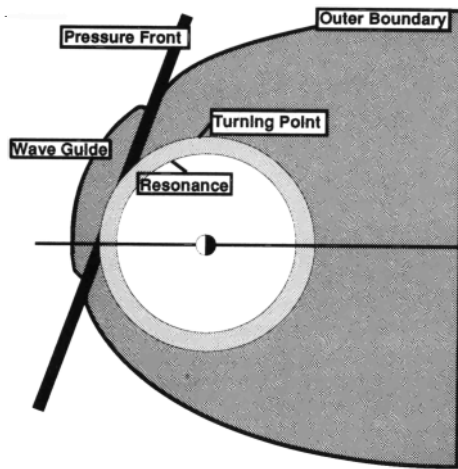


Fig. 1. A schematic of the MHD waveguide in the equatorial plane of the Earth's magnetosphere.

tion in which the resonances are driven by a monochromatic, compressional "pump." An important aspect of our study is that we treat the full set of MHD equations, not the linearized equations used in other studies [Allan *et al.*, 1986; Inhester, 1987; Lee and Lysak, 1991]. Consequently, we are able to deal with possible nonlinear effects which might be expected in the vicinity of the resonance, where the wave fields can rapidly become large. To the best of our knowledge, the results presented here represent the first fully three-dimensional treatment of the nonlinear evolution of FLRs driven by compressional Alfvén waves.

The results presented in this paper do not include kinetic effects, nor is there any background "noise" which would act as a seed for the resonances to form Kelvin-Helmholtz vortices in the equatorial plane [Rankin *et al.*, 1993] when the resonances have grown to large amplitude. These simulations are left for future

studies, as they add considerable complexity to an already complicated situation. Our results show that with simulation parameters compatible with the measured characteristics of 1- to 4-mHz FLRs in the auroral ionosphere, the FLRs narrow rapidly enough to allow the possibility of kinetic effects after only a few cycles in the wavetrain. Our simulations suggest that kinetic effects are likely to be important in FLRs occurring in the Earth's magnetosphere.

BASIC EQUATIONS AND LINEARIZED SOLUTIONS

The basic configuration we are attempting to model is shown in Figures 1 and 2. A solar wind pressure pulse causes a disturbance to propagate antisunward along the magnetopause boundary. The disturbance on the boundary layer excites compressional waves, which travel toward the Earth until they encounter their turning points. Most of the incident compressional wave energy is reflected at the turning point, but part of it tunnels toward the resonance point where the FLR is excited. In what follows, we examine the excitation of FLRs which have turning points on *L* shells situated at 8 to 10 *R_E* in the equatorial plane. Although the incident waves are broad band, only certain discrete frequencies can produce the FLRs which are observed [Harrold and Samson, 1992]. This is due to MHD cavity modes being formed between the turning points and the outer boundary, possibly the magnetopause.

Figure 2 shows the geometry of a FLR as described in our Cartesian box model of the magnetosphere. An incident fast-mode wave impinges on the plasma from the direction of the magnetopause boundary. The fast mode is refracted by the gradient in the Alfvén velocity until it reaches its turning point, where it is partly reflected. At the resonance location, the evanescent field excites a shear Alfvén wave, which is confined along the field line on the earthward side of the turning point. The shear waves reflect from the ionospheres, and set up a standing wave profile with a large azimuthal magnetic field (*B_y*, component) antinode (node) at the ion-

Geometry of a Field Line Resonance

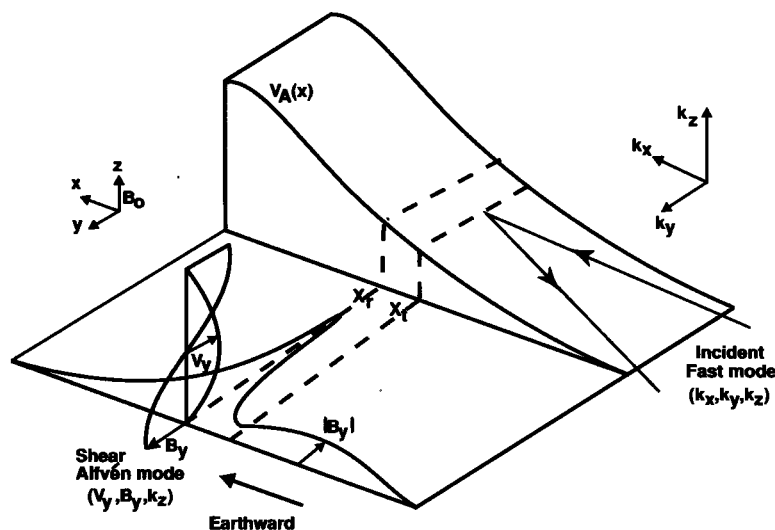


Fig. 2. Geometry of a FLR in a box model magnetosphere. The figure shows a fast mode impinging on a plasma from the direction of the magnetopause. Coordinate *x* measures radius, *y* is azimuthal, and *z* is the field-aligned direction. The Alfvén velocity profile varies approximately as $v_A(x) = v_R(x_R/x)^3$ in the vicinity of the FLR (with $v_R \sim 500$ km/s and $x_R \sim 8$ to $10 R_E$) and plateaus in order to accommodate boundary conditions described in the text. This dependence of the Alfvén profile is valid within a region $L_x \sim 1 R_E$ centered around the resonance position.

ospheres (equator) and a velocity field (v_y component) antinode (node) at the equator (ionospheres). The plateau in the Alfvén velocity profile is for numerical purposes only and is used to accommodate the boundary conditions to be discussed later.

The coupling of MHD compressional wave energy to FLRs is described by the full set of magnetohydrodynamic equations

$$\frac{\partial \rho}{\partial t} + \nabla \cdot (\rho \mathbf{v}) = 0 \quad (1)$$

$$\frac{\partial}{\partial t} \rho \mathbf{v} + \nabla \cdot (\rho \mathbf{v} \mathbf{v}) + \nabla P + \frac{1}{\mu_0} \mathbf{B} \times (\nabla \times \mathbf{B}) = 0 \quad (2)$$

$$\frac{\partial \mathbf{B}}{\partial t} - \nabla \times \left[\mathbf{v} \times \mathbf{B} - \frac{\eta}{\mu_0} \nabla \times \mathbf{B} \right] = 0 \quad (3)$$

$$\frac{\partial P}{\partial t} + \gamma \nabla \cdot (P \mathbf{v}) - (\gamma - 1) \left[\mathbf{v} \cdot \nabla P - \frac{\eta}{\mu_0^2} (\nabla \times \mathbf{B})^2 \right] = 0. \quad (4)$$

Equations (1) to (4) describe the evolution of the plasma density, momentum, magnetic field, and pressure, respectively. All symbols have their usual meanings. Equation (4) for the pressure was obtained by making use of the energy equation for the plasma and the equation of state. The above system of equations is solved numerically in a Cartesian geometry by using an alternating-direction-implicit method [Rankin *et al.*, 1993]. The implicit method is necessary in order to avoid restrictively small timesteps and to ensure numerical stability when large gradients in the Alfvén velocity are encountered.

The numerical solution of the nonlinear set of equations above will be compared with the results of linear theory. Noting that the ambient magnetic field and plasma density are inhomogeneous in the x direction (x corresponds to the radial direction), the linearization of the magnetohydrodynamic equations (1) to (4) above leads to a system of two equations which describe the spatial variation of the plasma pressure and displacement associated with the mode conversion of Alfvén waves,

$$\frac{dP_T}{dx} = \rho_0 \left[\omega^2 - k_z^2 v_A^2 \right] \xi_x \quad (5)$$

$$\frac{d\xi_x}{dx} = \frac{-G(x)}{\omega^2 - k_z^2 v_A^2} \frac{P_T}{\rho_0}. \quad (6)$$

In deriving these equations, we have allowed for gradients in the x direction and have assumed solutions of the form $\xi(x, y, z) = \xi(x) \exp[i(\omega t - k_y y - k_z z)]$, where ξ is the plasma displacement and P_T is the total perturbation pressure associated with the waves; i.e., $P_T = p + B_0 b_z / \mu_0$. The function $G(x)$ is defined by

$$G(x) = \frac{\omega^2 \left[\omega^2 - (k_y^2 + k_z^2) v^2 \right] + k_z^2 (k_y^2 + k_z^2) v_s^2 v_A^2}{\omega^2 v^2 - k_z^2 v_s^2 v_A^2} \quad (7)$$

in which v is given by $v^2 = v_A^2 + v_s^2$, where v_A is the Alfvén speed and v_s is the sound speed. Substitution of (5) into (6) leads to the equation

$$\frac{d^2 \xi_x}{dx^2} + \frac{1}{F} \frac{dF}{dx} \frac{d\xi_x}{dx} + G \xi_x = 0 \quad (8)$$

in which F is defined by

$$F = \rho_0 \frac{(\omega^2 - k_z^2 v_A^2)}{G}. \quad (9)$$

Equation (8) has two turning points at positions x_t for which $G(x_t) = 0$ and two resonances at positions x_r for which $F(x_r) = 0$.

The latter correspond to the shear Alfvén resonance, $\omega^2 - k_z^2 v_A^2 = 0$, and the cusp resonance, $\omega^2 v^2 - k_z^2 v_A^2 v_s^2 = 0$.

In the vicinity of the shear Alfvén wave resonance, where $\omega^2 / v_A^2 - k_z^2 = 0$, the plasma may be considered to be cold, and $G = \omega^2 / v_A^2 - (k_y^2 + k_z^2)$. These approximations enable (8) to be written as

$$\frac{d^2 \xi_x}{dx^2} + \frac{1}{(x - x_r + i\gamma)} \frac{d\xi_x}{dx} - k_y^2 \xi_x = 0, \quad (10)$$

in which the imaginary term $i\gamma$ takes into account losses in the system,

$$\gamma = \frac{\text{Im} \{ \epsilon(x_r) \}}{\frac{d}{dx} \text{Re} \{ \epsilon(x_r) \}}, \quad (11)$$

where $\text{Re} \{ \epsilon \} = \omega^2 / v_A^2 - (\text{Re} \{ k_z \})^2$. The solution to (10) is given by

$$\xi_x = \xi_0 \ln [k_y (x - x_r + i\gamma)]. \quad (12)$$

The overall spatial variation of the fields can be determined by matching (12) with the outer WKB solutions of (8) and the Airy function solution, which is valid at the turning point. The loss term in (12) removes the singularity at the resonant point and determines the radial scale size of the FLR. To get an estimate for the expected scale size of the FLR, it is therefore necessary to consider the losses in more detail. If we assume that losses are due to processes taking place in the ionosphere, where there is a finite height-integrated Pedersen conductivity, Σ_p , then k_z will be complex: $k_z = \text{Re} \{ k_z \} + i \text{Im} \{ k_z \}$, with $\text{Re} \{ k_z \} \approx m \pi / 2L$, where $2L$ is the effective length of the field line. The term $\text{Im} \{ k_z \}$ determines the losses.

To estimate the radial scale size of the FLR, we will use (12), and the boundary conditions at the ionospheres. Assuming that the shear Alfvén waves form a standing wave along z , we can write their E_x electric field component in the form

$$E_x(z, t) = E_0 \left[e^{i(k_z z + \Phi)} + e^{-i(k_z z + \Phi)} \right] e^{-i\omega t} \quad (13)$$

and note that at the ionospheres the following relationship applies:

$$\mathbf{B} \times \mathbf{z} = \pm \mu_0 \Sigma_p \mathbf{E}, \quad (14)$$

where the \pm signs refer to the northern and southern ionospheres, respectively, and where Σ_p represents the height-integrated Ped-

ers conductivity at the ionospheres. Using (14) and the relationship between E and B from Maxwell's equations, we can write down the following equation for the fields at the ionospheres:

$$\frac{1}{i\omega} \frac{\partial E_x}{\partial z} \pm \mu_0 \Sigma_p E_x = 0. \quad (15)$$

A straightforward application of (13) and (15) leads to expressions for the real and imaginary parts of k_z , and for the phase factor Φ ,

$$\begin{aligned} \text{Im} \{k_z\} &= \frac{-\ln|R|}{2L} \\ \text{Re} \{k_z\} &= \theta + \frac{n\pi}{2L} = \frac{m\pi}{2L} \\ \Phi &= \frac{i}{2} \ln|R| - \frac{\theta}{2} - n\pi \end{aligned} \quad (16)$$

where $|R|$ and θ are the amplitude and phase, respectively, associated with the reflectivity of the ionospheres:

$$R = |R| e^{i\theta} = \frac{\Sigma_m - \Sigma_p}{\Sigma_m + \Sigma_p}. \quad (17)$$

In (17), $\Sigma_m = 1/\mu_0 v_A$ represents the conductivity associated with the shear Alfvén waves. Using (12), the radial dependence of E_x in the vicinity of the FLR may be shown to be

$$E_x(x) = \frac{ik_y E_0}{(\text{Re} \{ \varepsilon \} - k_z^2)(x - x_r + i\gamma)}. \quad (18)$$

Taking the modulus and noting that near to the FLR $\omega^2/v_A^2(x) - k_z^2 \ll k_y^2$, it is easily seen that E_x may be approximated as

$$\frac{|E_x|}{E_0} = \frac{1}{k_y} [(x - x_r)^2 + \gamma^2]^{-1/2}. \quad (19)$$

In a similar fashion, (11), (16) and (17) can be used to find the following expression for the imaginary term γ :

$$\gamma = -\frac{\ln|R|}{\pi} \left(\frac{1}{v_A} \frac{dv_A}{dx} \right)^{-1} \Big|_{x=x_r} = \frac{x_r}{3\pi} \ln|R| \quad (20)$$

where $v_A(x) = v_0(x_0/x)^3$ has been assumed. From (20), the half-width-half-maximum of the FLR can then be evaluated as

$$|x_h - x_r| = \frac{x_r}{\pi\sqrt{3}} \ln|R|. \quad (21)$$

This latter expression enables us to estimate the radial width of the FLRs, given values for the reflectivity R and the particular L shell on which the resonances are situated. For example, a typical nightside ionospheric value for Σ_p near to quiet arcs is greater than 20 mho, whereas 10 to 20 mho is typical of diffuse aurora. Above the ionosphere, v_A is typically 10^4 km/s, giving $\Sigma_m \sim 0.1$ mho, and thus for $\Sigma_p = 10$ mho we find that

$|R| = 0.99$. Examining the L shell for which $x_r = 10R_E$, we find that the full-width-half-maximum (FWHM) of such a FLR is approximately 240 km, i.e., approximately $0.04 R_E$. These values are to be compared with the gyroradius of a ~ 10 -keV proton, which has been adiabatically heated as it convects toward the Earth from the magnetotail. For such a proton, the gyroradius is on the order of hundreds of kilometers and thus our estimates of the width of the resonances indicate that kinetic effects should be important provided that the resonances can narrow rapidly enough and that nonlinear processes do not "broaden" the resonances [Rankin et al., 1993]. In order to examine this in more detail, we turn to numerical solutions of the MHD equations.

FAST MODE DRIVER AND BOUNDARY CONDITIONS

In order to resonantly excite shear Alfvén wave FLRs, we must have a source of compressional MHD wave energy. In the simulations this is accomplished by specifying an incident harmonic wave field on the boundary of the system. The y - z plane at $x = 0$ represents a boundary in which a source of fast-mode Alfvén waves is incident on the boundary as a result of, for example, solar wind pressure pulses impinging on the magnetospheric cavity. We assume that the fast-mode waves are monochromatic in order to simplify the boundary conditions. This is a reasonable approximation since the FLRs of interest are cavity modes and have quantized frequencies [Kivelson and Southwood, 1986]. The wave fields on the boundary are chosen to satisfy the linear dispersion relation for a warm plasma. The form of the dispersion relation may be obtained from the linearized MHD equations (5) and (6) above by replacing derivatives with respect to x by ik_x . For the compressional waves, this leads to a dispersion relation of the form

$$\omega^4 - \omega^2 k^2 (v_A^2 + v_s^2) + k^2 k_z^2 v_s^2 v_A^2 = 0. \quad (22)$$

This equation has two solutions for ω^2 . The positive square root is the solution corresponding to the fast mode,

$$\omega^2 = \frac{k^2 (v_A^2 + v_s^2)}{2} \left(1 + \sqrt{1 - \frac{4v_s^2 v_A^2 k_z^2}{(v_A^2 + v_s^2)^2 k^2}} \right). \quad (23)$$

If the parameters on the right hand side of (23) are specified at $x = 0$, the frequency of the driver wave is determined. Knowing the frequency, the wave fields on the boundary can then be specified. The simulation code advances the eight main variables, B , v , P , and ρ . The incident wave fields on the boundary are linear in the sense that their amplitude is small relative to the ambient field B_0 ($B_0 = 20$ nT in the simulations to be described below). Under this assumption, and using the fast-mode dispersion relation to eliminate the shear wave and the slow wave from the incident wave fields, a straightforward evaluation of the homogeneous linearized MHD equations leads to a set of relations which specifies the fields of the incident wave at $x = 0$,

$$b_x = \omega^{-1} \frac{k_x}{k_y} k_z E_x \quad (24)$$

$$b_y = \omega^{-1} k_z E_x \quad (25)$$

$$b_z = -\omega^{-1} \frac{k_{\perp}^2}{k_y} E_x \quad (26)$$

$$v_x = -B_0^{-1} \frac{k_x}{k_y} E_x \quad (27)$$

$$v_y = -B_0^{-1} E_x \quad (28)$$

$$v_z = -B_0^{-1} \frac{k_z}{k_y} \frac{k_{\perp}^2 v_s^2}{\omega^2 - k_z^2 v_s^2} E_x \quad (29)$$

$$\rho = -\omega^{-1} \frac{\rho_0 k_{\perp}^2}{B_0 k_y} \frac{\omega^2 v_s^2}{\omega^2 - k_z^2 v_s^2} E_x \quad (30)$$

In these equations, perturbed quantities appear on the left-hand side and B_0 and ρ_0 represent the ambient magnetic field and density at $x = 0$. The perturbed pressure may be evaluated from (30) by using the fact that for the wave fields, $p = v_s^2 \rho$. The driver electric field E_x at $x = 0$ is chosen to vary sinusoidally in time according to $E_x = E_0(t) \sin(\omega t - k_y y - k_z z + \Phi)$, where $E_0(t)$ is a function which varies linearly with time to some specified maximum value (corresponding to turning on the driver slowly) and Φ is a phase factor which depends on the reflection coefficient at the ionospheres.

Equations (24) to (30) specify field values corresponding to compressional driver waves incident on the boundary from outside of the system. However, in order to permit waves reflected from plasma gradients inside the system to leave the simulation box, outgoing wave conditions are required. Boundary conditions for this can be constructed as follows: Let $f(x, y, z, t)$ denote any one of the field variables corresponding to the waves, and note that f can be written as a superposition of waves traveling in the $+x$ (p) and $-x$ (m) directions, respectively. Thus,

$$f(x, y, z, t) = f_p(x - v_x t, y, z) + f_m(x + v_x t, y, z). \quad (31)$$

Differentiating these equations with respect to $\psi = x - v_x t$ and $\phi = x + v_x t$ leads to the following relationships:

$$\left(\frac{\partial}{\partial x} - \frac{1}{v_x} \frac{\partial}{\partial t} \right) f = 2 \frac{\partial f_p}{\partial \psi} \quad (32)$$

$$\left(\frac{\partial}{\partial x} + \frac{1}{v_x} \frac{\partial}{\partial t} \right) f = 2 \frac{\partial f_m}{\partial \phi}. \quad (33)$$

The operator on the left-hand side of (32) ignores waves moving to the left, letting them leave the system, and this is what is required at $x = 0$, for example, so that (32) at $x = 0$ can be rewritten as

$$\frac{\partial f}{\partial t} - v_x \frac{\partial f}{\partial x} = 2 \frac{\partial f_p}{\partial t}. \quad (34)$$

The time rate of change on the right-hand side of this equation is user specified and is essentially determined by (23). The amplitudes (f_p) of the incident wave fields are specified by (24) to (30).

The above form of boundary condition is adequate since the excited shear Alfvén waves are trapped in the resonance region inside the plasma and there is no flux of these waves across the boundary at $x = 0$. The above boundary condition is specified in space- and time-centered fashion for all of the main variables used in the MHD code. Boundary conditions are also required at $x = L_x$, the length of the system in the x direction. We simply use a reflecting boundary condition there. For numerical purposes, the form of the ionospheric boundary condition may be expressed using equations identical to (32) and (33), except that the arguments are now $\psi = z - v_z t$ and $\phi = z + v_z t$, respectively. At $z = 0$ we require $f_p = R f_m$, where R is the reflection coefficient at the ionosphere (cf(17)), and thus (32) and (33) imply that the wave field components at the ionospheres satisfy

$$(1 - R) \frac{\partial f}{\partial t} - (1 + R) v_z \frac{\partial f}{\partial z} = 0. \quad (35)$$

The boundary condition at $z = L$, which represents the equatorial plane, uses the symmetry of the field components: the magnetic field b_{\perp} is anti-symmetric at the equator, v_{\perp} is symmetric, v_z is anti-symmetric, and b_z is symmetric. In the y direction, periodic boundary conditions are used. In the simulation results which follow, the number of computational zones used corresponds to 100 in x , 48 in y , and 20 in z . The mesh is nonuniform in x , with a minimum spacing at the resonance position, and is uniform in the other two directions.

RESULTS

Coupling of MHD wave energy to FLRs may be characterized by the parameter shown below [Kivelson and Southwood, 1986; Inhester, 1987],

$$q = \frac{k_y^2}{(-k_z^2 v_A^2 \frac{d}{dx} v_A^{-2})^{2/3}}. \quad (36)$$

The fractional energy loss per wave cycle is in the range 40 to 50% at the resonance point when q is in the range 0.25 to 0.75. In the simulations we choose the parameters k_y and k_z such that $q \approx 0.5$. This places the coupling coefficient near to its optimum value. In reality, there is likely to be present a spectrum of incident wave angles, but the coupling will be the most efficient when $q \approx 0.5$. Larger or smaller values of q will imply growth of the FLR over a greater interval of time and perhaps a smaller saturation amplitude.

The ambient parameters are chosen for comparison with the cavity mode FLRs discussed by Harrold and Samson [1992]. The reader is referred to that paper for a detailed discussion, and in particular Figures 2c to 2d of the paper are used to estimate ambient quantities at the position of the FLR in the equatorial plane. Our results are appropriate to a region centered around the location of a 1.3-mHz FLR at an approximate radial distance of 8 to 10 R_E in the equatorial plane. In the vicinity of the FLR, the geomagnetic field strength is approximately 40 nT, the ambient density is between 2 and 3 particles/cm³, and the plasma temperature at $x = 0$ is 1.4 keV ($x = 0$ is on the anti-earthward side of the FLR). The Alfvén velocity profile (Figure 2) has an approximate $1/x^3$

variation in the vicinity of the FLR ($v_A \sim 500 \text{ km/s}$ at the FLR location), and the ambient density increases from the resonance position toward $x = 0$ in order to accommodate pressure balance (the density increases by a factor of three). The density is varied in this manner in order to avoid unrealistically high plasma temperatures at $x = 0$ as a result of the demand for pressure balance. This results from our choice of a Cartesian geometry; in reality the field line curvature would lead to a more realistic pressure balance. Our results are not sensitive to these approximations, and in particular the local plasma conditions at the position of the FLR are critical since the resonance narrows to very short scales. The ambient profiles are uniform near to $x = 0$ and $x = L_x$ ($L_x \sim 1 R_E$) in order to accommodate the boundary conditions discussed earlier. The driver electric field $E_0(t)$ is specified in terms of the dimensionless parameter $E(t) = (1/v_{A0})E_0(t)/B_0$. This quantity is ramped up linearly with time to a constant value over a timescale comparable to the Alfvén transit time to the resonant point. Specifically, $E(t) = \min(t/\alpha T_0, E_{max})$, where $T_0 \sim L_x/v_{A0}$ is the Alfvén transit time, α is a dimensionless parameter which takes the value 0.2 in the results to be presented, and E_{max} is the maximum amplitude of the normalized field. We have used a growing waveform for simplicity in order to get fast-mode wave energy into the system. Impulsively generated global modes are likely to be decaying during part of the timescale for which field FLRs are being excited. However, the essential parameter is the amount of energy deposited in the resonance region, and it should be unimportant whether the excitation waves are growing or damping, provided they do not damp too rapidly.

In Figures 3 and 4 we show x - y cuts of the data for the magnetic field component B_y at three positions along z , $z = 0$ (just above the ionosphere), $z \sim L/2$, and $z \sim L$ (near to the equatorial plane). We take as our time unit the number of elapsed wave periods of the MHD driver and choose a value for the reflectivity at the ionospheres corresponding to $|R| = 0.95$. The maximum driver amplitude E_{max} at $x = 0$ corresponds to $B_{ymax}/B_0 = 0.05$ for this case. As discussed above, reflectivities corresponding $|R| = 0.99$ are more consistent with diffuse aurora. The lower reflectivity results being presented here are mainly by way of illustration. Figure 3 represents data output from the simulations after approximately 2 wave periods, and Figure 4 shows the data output after approximately 13 wave periods. It should be remembered that B_y has a node at the equatorial plane and an antinode at the ionosphere. The y -dependent sinusoidal nature of the driver field at the boundary $x = 0$ is evident in these figures, as is the excitation of a disturbance near to $x = L_x/2$. The latter represents the FLR which is secularly growing as a result of mode conversion of the fast-mode driver wave. It can be seen that the FLR also has the same sinusoidal y and z dependence as the driver wave (B_y has a node at the ionosphere, and an antinode at the equator), indicating that the FLR is being excited in the fundamental mode. The growth in the amplitude of the resonance saturates shortly after the time indicated in Figure 4, corresponding to approximately 14 to 15 wave periods. This occurs either as the result of nonlinear processes or as a result of the Poynting flux of the Alfvén waves through the ionospheres due to the finite conductivity.

The v_y velocity component is found to have an identically topological form to the B_y fields shown in Figures 3 and 4, except that v_y has a node at the ionosphere and an antinode at the equator. Figures 3 and 4 indicate that at early times the amplitude of the FLR is small and its width in the x direction is relatively large. As the wave amplitude grows, the FLR narrows rapidly with time. In Figure 5 (with $|R| = 0.95$), we show the temporal growth of the maximum value of B_y in the portion of the x - y plane at $z = 0$ which

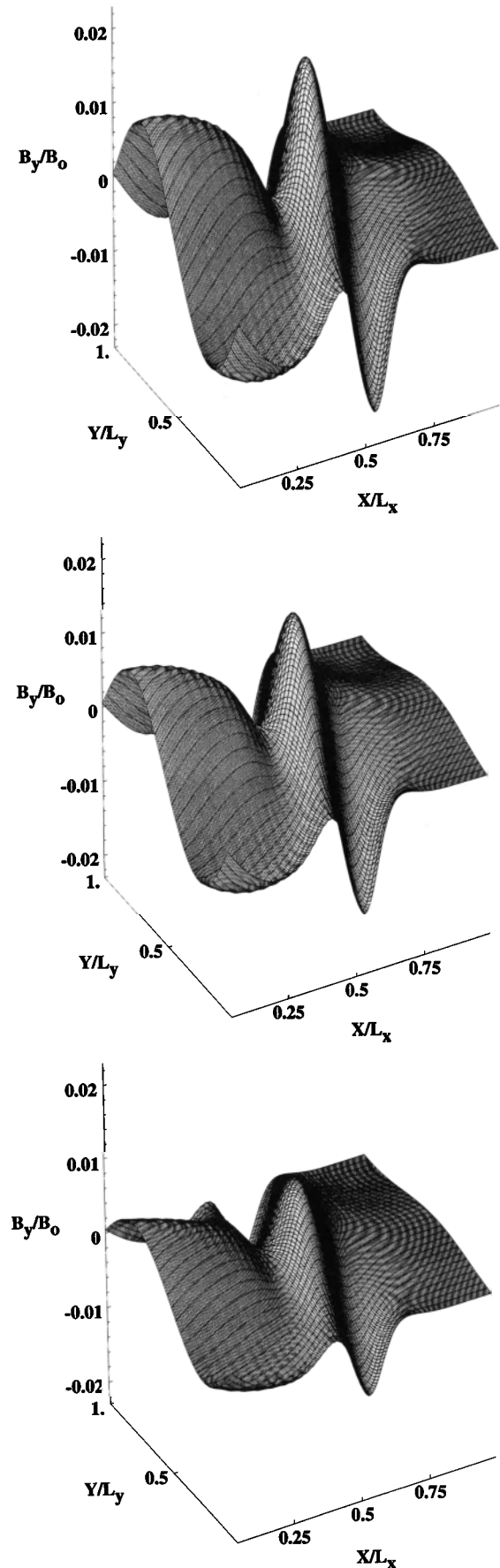


Fig. 3. B_y component of the wave magnetic field as a function of x and y for three positions along z . (a) near to the ionosphere $z = 0$, (b) $z \sim L/2$, (c) near to the equatorial plane $z \sim L$. The elapsed time corresponds to two wave periods of the incident MHD fast-mode driver.

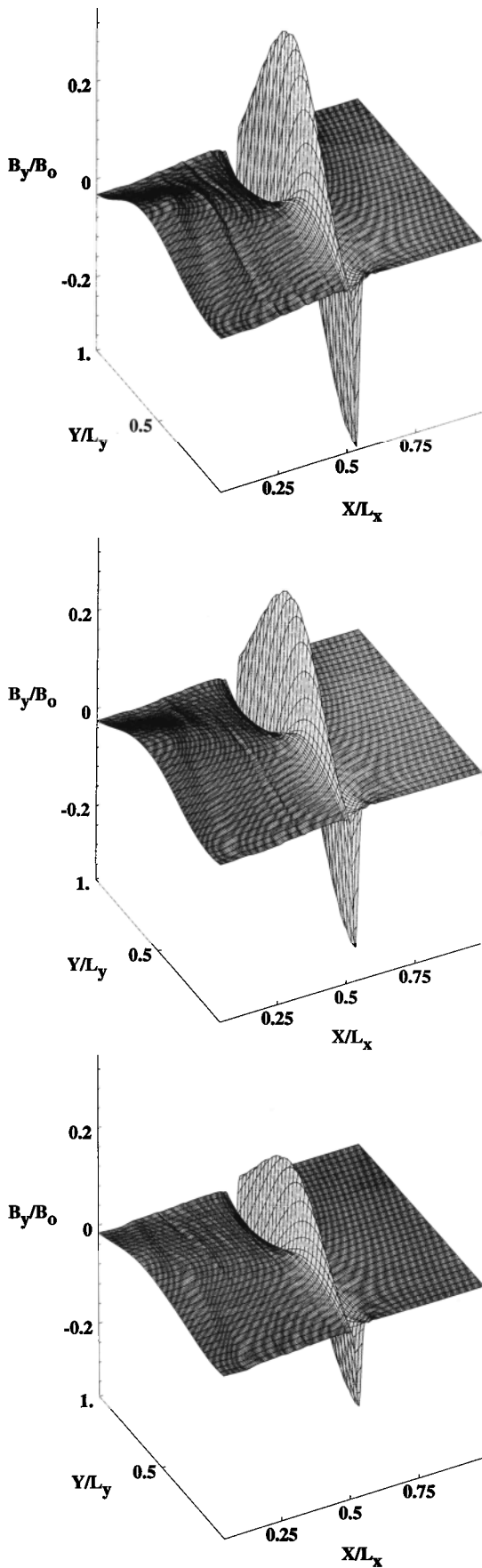


Fig. 4. B_y component of magnetic field as a function of x and y for three positions along z . (a) near to the ionosphere $z = 0$, (b) $z \sim L/2$, (c) near to the equatorial plane $z \sim L$. The elapsed time corresponds to 13 wave periods of the incident MHD fast-mode driver. The FLR saturates slightly after this stage in the evolution.

encompasses the FLR. As discussed above, saturation of the amplitude of the excited waves occurs after an elapsed time of approximately 14 wave periods. It can be seen that the peak amplitude of the B_y field of the FLR at saturation is approximately 0.35 times the value of B_0 on the boundary at $x = 0$ (B_0 is appropriate to values in the equatorial plane of the real magnetosphere), corresponding to roughly 18 to 20% of the ambient geomagnetic field value at the resonance position. The maximum azimuthal velocity of the resonance in the equatorial plane is very large, amounting to approximately 60 km/s after saturation. These velocities are compatible with measured values from satellites [Mitchell et al., 1990] and values inferred from radar measurements [Walker, 1980]. The large radial shear in the azimuthal velocities in the equatorial plane, 120 km/s across the resonance, makes the resonance susceptible to nonlinear effects such as Kelvin-Helmholtz (KH) instabilities. The consequence of these large velocity shears will be examined later.

An important result here is that the FLRs narrow to scales where kinetic effects might play a role after only several wave cycles, an interval which is much shorter than that suggested by Allan and Poulter [1989]. In the absence of ionospheric dissipation, these authors considered a mechanism termed dissipative phase mixing for determining qualitatively the timescale for which kinetic effects are likely to become important. The timescale they estimate relies on order-of-magnitude estimates of magnetic viscosity and resistivity and leads to the conclusion that hundreds of cycles would be required for coupling to kinetic Alfvén waves to become important. This is in contrast to the results of Inhester [1987], who concluded that kinetic effects might become important at earlier times owing to the very small damping of FLRs provided by a highly conducting ionosphere. In our three-dimensional model, damping is a natural consequence of the ionosphere, and the observational constraint of a highly reflecting ionosphere brings our predictions of timescales in accord with those of Inhester [1987]. We shall see later that nonideal MHD effects can become important when the scale size of the FLR is an order of magnitude larger than the scale lengths associated with electron inertia waves. Our calculations are in accord with observations of FLRs, which indicate that the actual evolution timescales are on the order of only a few wave periods [Walker et al., 1992]. We have also studied the evolution of FLRs when a smaller amplitude driver ($B_{y,max}/B_0 = 0.01$) is imposed at $x = 0$. The temporal evolution of the resonance is unaffected; i.e., growth and sat-

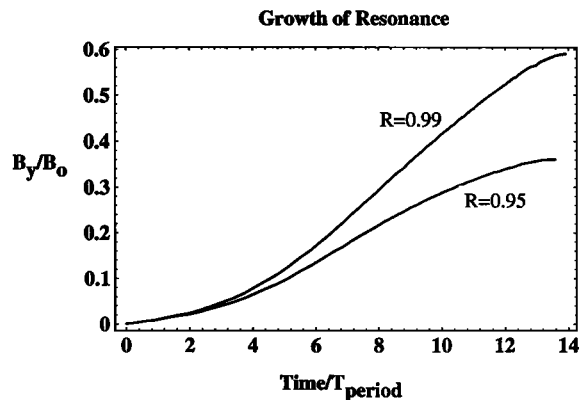


Fig. 5. Temporal growth of the maximum value of B_y in the portion of the x - y plane which contains the FLR. The data are sampled in the x - y plane near to the ionosphere, where the maximum fields occur. The peak amplitude of the FLR saturates after approximately 14 wave periods of the fast-mode MHD driver. The two curves correspond to ionospheric reflectivities $|R| = 0.99$ and $|R| = 0.95$, respectively.

uration occur after approximately 14 wave periods. However, the saturation amplitude of the B_y field of the resonance is smaller, amounting to roughly 8% of B_0 . This gives an approximate linear scaling of the amplitude of the FLR with the amplitude of the driver field, at least within the considered range of parameters. This is not unexpected, since saturation occurs when the ionospheric losses are balanced by the Poynting flux of the driver waves into the resonances.

In Figure 6, we show cuts of the data in the x - y plane near to the ionosphere ($z = 0$) at elapsed times corresponding to 2, 3, 8, and 14 cycles of the MHD driver. At early times, the FLR has an overall width of approximately $0.4 R_E$ and is observed to grow rapidly and narrow significantly over a time period of only three or four wave cycles. Using Figure 6 we estimate that the FWHM transverse scale size just as the structure saturates is near to $0.06 R_E$, i.e., in reasonable agreement with (21), although this agreement does not necessarily imply that the saturation mechanism determining the widths of the resonances can be attributed to linear processes.

In our Cartesian geometry, the scale sizes of the FLR do not change along the field lines. In particular, near to the ionosphere our scale sizes are actually overestimated by as much as a factor of 40 to 50 [Walker, 1980], reflecting the fact that in a dipolar geometry the geomagnetic field lines converge near to the ionosphere. Nevertheless, our calculations should be valid in the equatorial plane, where the highest-velocity fields are expected. Observationally, the scale sizes of the velocity fields of the resonances in the E and F regions of the ionosphere are 40 km or so [Samson *et al.*, 1992a, Walker *et al.*, 1992], and taking into account the mapping factor associated with the magnetic field convergence, this corresponds to a scale size in the equatorial plane of $\sim 0.4 R_E$. This is consistent with the early time results predicted by our simulations (for reflectivities between $|R| = 0.95$ to 0.99) but is significantly larger than the late time results when the resonances have grown to large amplitude. However, it is worth pointing out that the observational scale sizes are at the limits of the instrumentation and that narrower structures may in fact be forming. The 1 to 2 cycles narrowing time observed by Walker *et al.* [1992] may represent only a fraction of the time interval over which the FLRs narrow. The actual scale size which results from the mode conversion of a solar wind pressure pulse will depend on the amplitude and duration of the pulse, the conductivity of the ionospheres, and whether nonlinear processes, for example, nonlinear KH instabilities in the FLRs [Rankin *et al.*, 1993], or kinetic processes can prevent very small scale sizes from forming. However, within the framework of the resistive MHD equations, our results indicate that large amplitude FLRs can form relatively easily and that narrowing of the structures can occur within the observed lifetime (typically a few wave cycles) of MHD wave events.

The reflectivity of the ionosphere is a significant parameter affecting the amplitude and scale size of FLRs. To investigate this latter point, we have repeated the above calculation using a reflectivity which is consistent with that encountered in the high-latitude polar ionosphere, namely $|R| = 0.99$. Figure 5 also shows the growth of the FLR with time for this case. The wave fields grow more rapidly than for $|R| = 0.95$, reflecting the lower losses through the ionosphere, and saturation occurs at a higher amplitude, i.e., at approximately 0.55 to 0.60 times the ambient magnetic field value at the boundary $x = 0$ (again, in the real magnetosphere, these comparisons with B_0 are appropriate to values in the equatorial plane). The FLRs narrow more rapidly for this case,

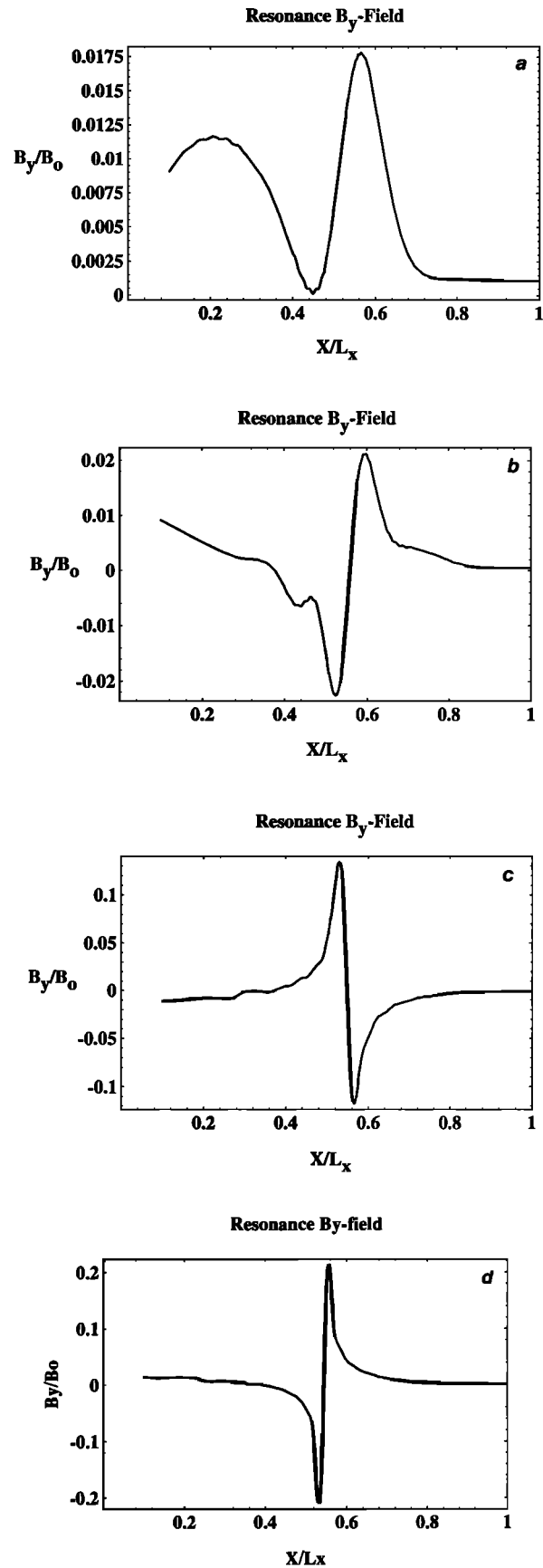


Fig. 6. A line from the B_y data in the x - y plane near to the ionosphere ($z = 0$). The elapsed time corresponds to 2 (a), 3 (b), 8 (c), and 14 (d) cycles of the fast-mode driver wave. The reflectivity of the ionosphere is $|R| = 0.95$.

and the scale size at saturation is somewhat smaller than in Figure 6d, i.e., the FWHM is approximately $0.03 R_E$ as indicated in Figure 7.

DISCUSSION

The results presented above indicate that large amplitude FLRs, with velocity shears on the order of 100 km/s, can be driven over relatively short timescales in the equatorial plane of the magnetosphere. It is remarkable that the large amplitudes and very short radial spatial scales of these structures do not lead to significant deviations from the predictions of linear analysis cf (21). For example, in Figure 8 we show the y - z Fourier amplitude (sampled at the x coordinate corresponding to the peak value of the field of the FLR) of the B_y component data after the FLR has saturated at an amplitude in the equatorial plane corresponding to approximately 0.30 to 0.35 times B_0 . The Fourier amplitude is calculated according to the formula

$$a(x) = \int a(x, y, z) \exp[-i(k_y y + k_z z)] dy dz. \quad (37)$$

The four peaks in Figure 8 correspond to the fundamental modes $\pm 2\pi/L_y$ and $\pm \pi/2L$, respectively. There is no indication that higher-wavenumber modes are becoming important, since they would lead to a broadening of the spectrum or the generation of additional peaks in k -space. This is true for the higher reflectivity results also.

The two basic wave modes associated with mode conversion, i.e., the compressional and the shear wave, can also be investigated using a Fourier analysis of the simulation data. For the case here, mode conversion leads to a large growth in the amplitudes of B_y and v_y and only a small enhancement of B_x and v_x , as can be seen on examining the linearized MHD equations. The magnetic field component B_z is specific to the compressional wave and should vanish in the region where shear Alfvén FLRs are excited. On the other hand, compressional waves do not carry a field-aligned current, whereas shear Alfvén waves do. Therefore, J_z should be strongly peaked in the vicinity of the FLR where shear Alfvén waves are being excited. For example, in Figure 9 we show the evolution of the Fourier amplitude of the B_y component fundamental mode as a function of x and time. It can be seen that the mode amplitude is largest at the FLR position and that the fundamental mode becomes increasingly confined to the resonance location as its amplitude increases with time. The resonance is seen to be narrow over most of the evolution timescale. There are no

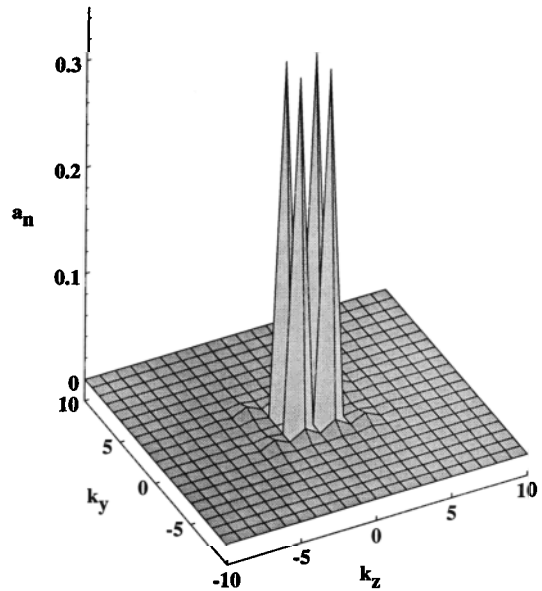


Fig. 8. Fourier transform of the B_y -component data (normalized to B_0) after the FLR has saturated at an amplitude corresponding to approximately 0.35 times B_0 . The four peaks correspond to the fundamental modes $\pm 2\pi/L_y$ and $\pm \pi/L$, respectively.

other significant wavenumber modes excited in the vicinity of the FLR, and in particular the amplitude of the next higher-order wavenumber mode is almost two orders of magnitude smaller than that of the fundamental mode shown in Figure 8. A time slice along the sharp ridge in Figure 9 can be compared with the corresponding curve shown in Figure 5, which contains information from all of the wavenumber modes which are present in the system. The differences between these two curves are found to be less than 2%. Clearly, the saturation amplitude of the FLR is due to the finite Poynting flux into the dissipative ionosphere (as a result of the finite conductivity), which just balances the Poynting flux into the FLR from the compressional pump.

Figure 10 shows the change in the phase of the B_y component of the wave across the FLR. The phase change of π predicted by linear theory and observed experimentally is clearly present. To calculate the phase of the waves, we have assumed that the wave profiles do not change in the z direction, which is correct because

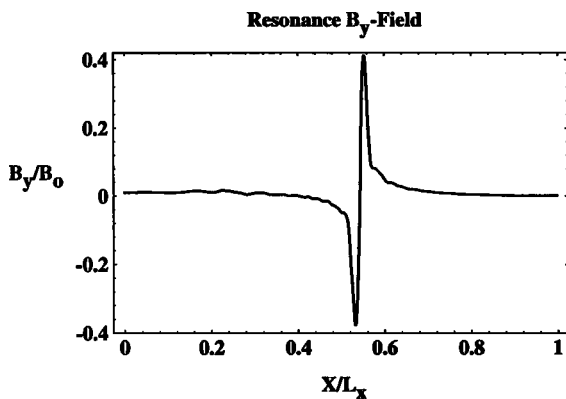


Fig. 7. A line from the B_y data in the x - y plane near to the ionosphere ($z = 0$). The elapsed time corresponds to 14 cycles of the fast-mode driver wave. The reflectivity of the ionosphere is $|R| = 0.99$.

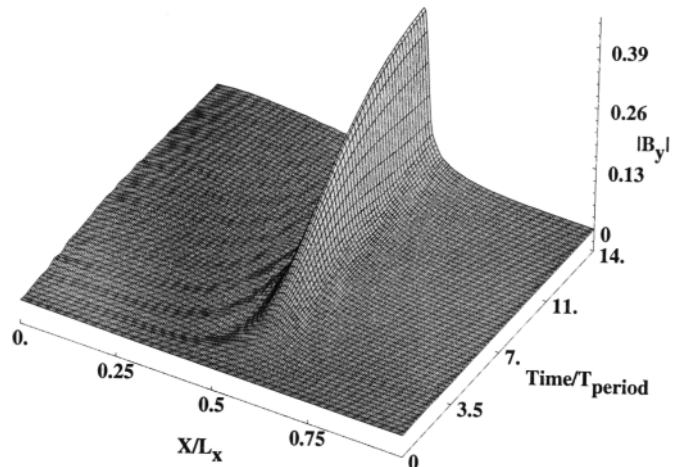


Fig. 9. Evolution of the Fourier amplitude of the B_y component fundamental wave mode (normalized to B_0) as a function of x and time.

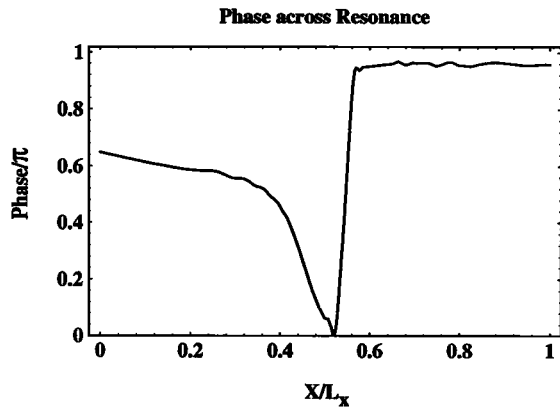


Fig. 10. Change in phase of the B_y component across the FLR.

the fields are standing waves along z . The phase can then be defined in terms of the phase of the Fourier amplitude,

$$a(x) = |a(x)| \exp[i \text{ phase}(x)], \quad (38)$$

and so we see that the phase determines the sign of a field quantity. As the resonance is traversed, the phase of B_y changes by π but there is no significant change in the phase of B_x , which means that the polarization is reversed in crossing the resonance point.

The compressional mode can also be investigated. For example, in Figure 11 we show the evolution of the fundamental mode amplitude associated with B_z . This field component is specific to the compressional mode, and it can be seen that B_z vanishes rapidly across the FLR location, emphasizing the absorption of energy from one wave type to the other as a result of mode conversion. An interesting feature present in Figure 11 is the temporal modulation of the data on the antiearthward side of the FLR. These modulations are spaced at intervals of the Alfvén wave period. At present these modulations remain an unexplained feature of the data. They are in fact present in all of the field components but are made clear in Figure 11 because the amplitude of B_z is small.

The field-aligned current J_z associated with the fundamental mode of the shear Alfvén waves is displayed in Figure 12. This quantity should be zero toward the boundary $x = 0$ (where the waves are essentially compressible) and should have a strong peak in the vicinity of the FLR which narrows with time. This behavior

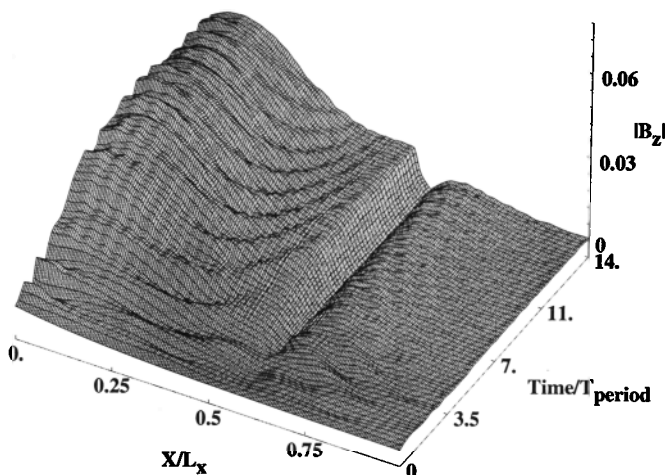


Fig. 11. Evolution of the B_z -component Fourier amplitude of the fundamental wave mode (normalized to B_0) as a function of x and time. B_z is a quantity specific to compressional Alfvén waves.

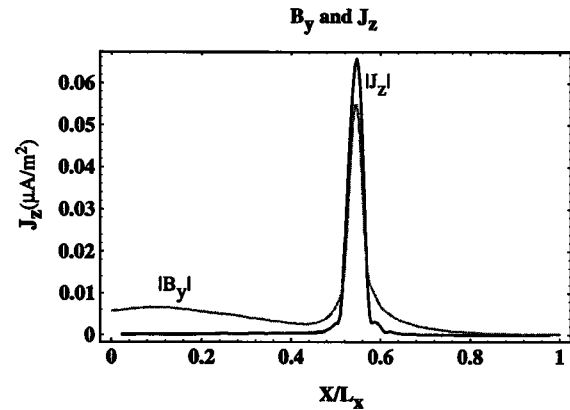


Fig. 12. The Fourier amplitude (fundamental mode) of the field-aligned current J_z as a function of x at a time when the amplitude of the FLR is almost saturated. J_z is a quantity specific to shear Alfvén waves. The units for B_y are arbitrary.

is observed in the simulations, and in Figure 12 it is clear that J_z is nonzero only across the resonance region. Also shown in Figure 12 is the corresponding field component B_y (scaled such that J_z and B_y can be displayed on the same figure). The transition from one mode to the other is clear in Figure 12; this also serves to indicate that processes are being modeled correctly. When the growth in the amplitude of the FLR is saturated, the field-aligned current corresponds to $J_z \sim 0.07 \mu\text{A}/\text{m}^2$. Again, taking into account geometrical mapping factors, in the actual magnetosphere this corresponds to current densities exceeding $3 \mu\text{A}/\text{m}^2$ near to the ionosphere, which is probably large enough to give rise to auroral arcs.

For completeness, we show the evolution of the B_x fundamental mode amplitude in Figure 13. This component is common to both the shear and compressional modes. Although it is not clear from this figure, it can easily be demonstrated that the peak B_x field in the vicinity of the FLR is growing over the time interval shown on the figure, even though B_x on the antiearthward side has reached steady state. The incoming and reflected compressional waves on the antiearthward side reach steady state relatively early in the simulation, after the incoming wave amplitude has been ramped up in time to its constant value.

The large velocity shears that are observed in the simulations should be sufficient to drive KH instabilities in the equatorial plane of the FLR. For example, the growth rate for the KH instability [Walker, 1981], assuming a discontinuous change in velocity across the region of velocity shear, is given approximately by $\omega_i = k_{y0} v_0$, where k_{y0} represents the wavenumber of the instability and v_0 represents the amplitude of the velocity shear region. Taking $v_0 = 80$ to 100 km/s , and a value for k_{y0} appropriate to a hyperbolic-tangent velocity shear region, for which maximum growth is determined by $k_{y0} \Delta \sim 0.6$, where 2Δ is the width of the velocity shear region, it is easily calculated that exponential growth times for the KH instability are on the order of 70 to 80 s for scale sizes corresponding to $\Delta \sim 0.1 R_E$. These timescales are much shorter than the observed periods of the FLRs, which are typically hundreds of seconds. The KH instability does not occur in the simulations owing to the absence of a small seed component of velocity having an appropriate wavelength for growth. We have seen that the absence of nonlinear effects in the simulations pre-

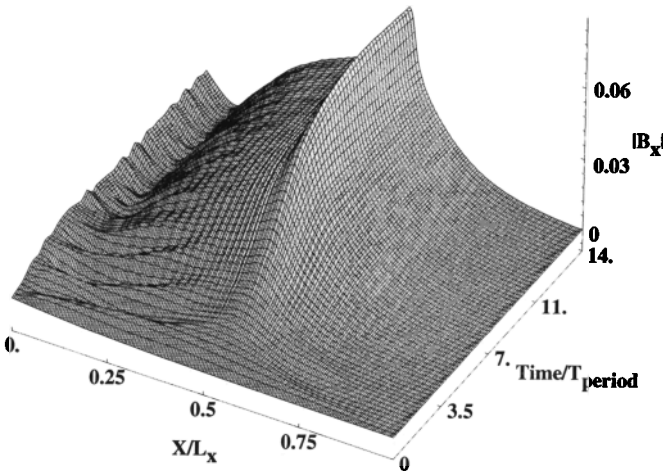


Fig. 13. Evolution of the B_x -component Fourier amplitude of the fundamental wave mode (normalized to B_0) as a function of x and time.

vents significantly higher k -modes from occurring. The wave numbers for growth of the KH instability are much larger than the k_y of the FLR [Samson *et al.*, 1992a, 1992b], and thus the instability cannot easily occur in the simulations. It is possible to artificially include a seed for the instability; however, a large increase in the number of computational mesh points in the y direction is required since the wavelength of the instability is much shorter than the corresponding azimuthal wavelength of the FLR. This places significant demands on computational resources and is deferred for future study. Rankin *et al.* [1993] have shown that the occurrence of KH instabilities in a simple model of FLRs can lead to broadening of the resonances as a result of formation of nonlinear vortex structures. However, their simplified model neglected coupling to the MHD driver and omitted the azimuthal structure of the FLR and the radial dependence of the ambient parameters.

In using the resistive MHD equations (1) to (4), we have of course neglected the finite Larmor radius of ions and the finite inertia of electrons. Corrections for these quantities become important when the characteristic length scale perpendicular to the ambient magnetic field becomes small. In the context of FLRs, ion Larmor radius effects are dominant near the equatorial plane when the electron thermal speed is greater than the Alfvén speed [Hasegawa, 1976], whereas at high latitudes the electron inertia length ($\lambda = c/\omega_{pe}$) is considerably greater than the ion gyroradius. In particular, we have seen that the radial scale sizes of FLRs in the equatorial plane can be smaller than the ion gyroradius of adiabatically heated protons convecting in from the magnetotail, and if we use the mapping factor discussed by Walker [1980], which accounts for the converging magnetic field topology in a dipolar magnetosphere, we find that the scale sizes of the FLR can be on the order of a few kilometers above the ionosphere. The scale sizes at the ionosphere are therefore comparable to the electron inertial length, and our MHD model should be modified to include finite electron inertia terms in the generalized Ohm's law. These corrections modify the dispersion relation of shear Alfvén waves, which become dispersive and are referred to as electron inertia Alfvén waves. Electron inertia waves induce parallel electric fields, which might lead to the formation of potential structures and the downward acceleration of electrons above the ionosphere [Seyler, 1990]. The precipitating electrons may modulate the conductivity of plasma near to the ionosphere and play a role in the dynamics of discrete aurora [Goertz, 1984].

Though a fully nonlinear treatment of mode conversion to electron inertia shear Alfvén waves is beyond the scope of the present

study, we can obtain some ideas about the possible effects of these waves by looking at numerical solutions to a set of linearized resistive MHD equations which has been derived using an Ohm's law which includes electron inertia effects in the direction of the magnetic field lines:

$$(\mathbf{E} + \mathbf{v} \times \mathbf{B} - \eta \mathbf{j}) \cdot \hat{\mathbf{z}} = \lambda^2 \mu_0 \frac{\partial \mathbf{j}}{\partial t} \cdot \hat{\mathbf{z}}. \quad (39)$$

To solve the equations, which will be described elsewhere, we assume that the plasma is cold and that the y and z dependences are of the form $\exp(ik_y y) \exp(ik_z z)$. We keep the dependence on the x coordinate as the plasma is inhomogeneous in this direction. The analysis results in a set of five equations which describe the evolution of the complex mode amplitudes in the x - t plane. We solve these equations numerically using a simple finite-difference scheme. The physical configuration is analogous to the nonlinear case presented above; i.e., a compressional pump wave enters the plasma and excites a FLR at the resonance point. For simplicity, we assume that the z -component ambient magnetic field is constant and that the Alfvén velocity gradient varies linearly across the resonance region owing to variations in the background density.

In Figure 14, we show the B_y magnetic field component of the waves with and without the inclusion of finite electron inertia. The amplitude of the FLR is smaller when finite electron inertia is included, and the resonance is more spatially structured because of the dispersive nature of the waves. We also observe a shift of the peak of the FLR to the right. For a fixed k_z , this shift is due to the dispersive effects which lower the frequency of the electron inertia waves: $\omega^2 = k_z^2 v_A^2 / (1 + k_\perp^2 \lambda^2)$, where k_\perp is the perpendicular wave number. The term in the denominator is larger than unity, and therefore the resonant point occurs at a higher Alfvén velocity, which in this case corresponds to a shift to the right toward lower density. The finite-gyroradius kinetic Alfvén wave experiences an analogous shift but in the opposite direction as its dispersion relation is $\omega^2 = k_z^2 v_A^2 (1 + k_\perp^2 r_g^2)$, where r_g is a gyroradius based on a combination of electron and ion temperatures. The propagation of the electron inertia wave away from the resonance position leads to an additional loss term, which results in a smaller saturated amplitude for the FLR than is predicted by the resistive MHD equations. Here, it should be noted that when finite electron inertia

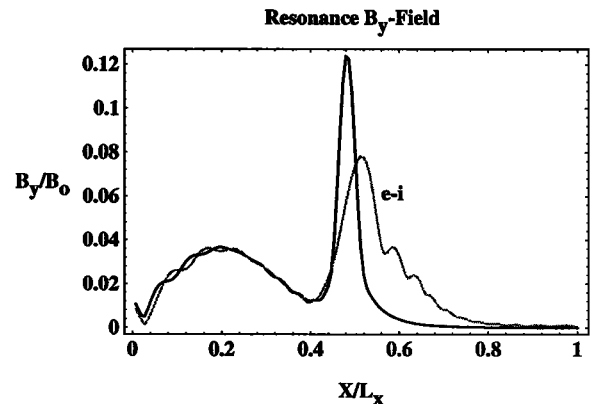


Fig. 14. B_y magnetic field component of the waves as a function of x when finite electron inertia effects are omitted (dark line) and when they are included (curve labeled e-i). The figure is for a cold plasma with a linear gradient in the Alfvén velocity.

effects are absent, saturation in the linear equations is possible because of the assumed constant resistivity of the plasma.

The electron inertia effect clearly leads to a broadening of the FLR in Figure 14, and consequently we would expect actual FLRs to have widths greater than those that have been estimated using our nonlinear MHD simulations. Our preliminary calculations show that with finite electron inertia effects, the FLR narrows to a width that is roughly 10 times larger than the local value of λ and that the final state is a stationary one in which the absorption of energy at the resonance point is balanced by energy emitted from the resonance in the form of Alfvén waves which propagate towards lower density plasma. Taking $0.1 R_E$ as a typical scale size in the equatorial plane for the FLRs predicted by our nonlinear MHD simulations, we estimate that the corresponding scale sizes at the ionosphere are on the order of 10 km, and since the electron inertial length near to the ionosphere is approximately 1 or 2 km, finite electron inertia effects should have a strong influence on the nonlinear evolution of FLRs in the Earth's magnetosphere.

CONCLUSIONS

Our simulations indicate that large-amplitude FLRs, with velocity shears on the order of 100 km/s, can be excited in the equatorial plane of the Earth's magnetosphere. The scale sizes of the FLRs, and the timescales for narrowing of the resonances to occur, are compatible with observations of FLRs in the high latitude polar ionosphere [Walker et al., 1992]. Narrowing of the resonances occurs within only a few cycles of the Alfvén wave train, and the radial scale size can approach $0.1 R_E$ when the amplitudes of the FLR have saturated. The scale sizes of the resonances in the equatorial plane are comparable to the ion gyroradius, and accounting for magnetic field convergence near to the ionospheres, the scale sizes there are comparable to the electron inertia length. This leads us to the conclusion that in order to examine FLRs in the 1- to 4-mHz range, the generalized Ohm's law in the MHD equations must be modified to include kinetic effects or effects due to finite electron inertia. In fact, we expect that kinetic effects will lead to resonances which are broader than the $0.1 R_E$ value found in these studies, since kinetic effects can begin to damp the resonance when the resonance scale size is comparable to the gyroradius or electron inertial length. We have modified our MHD model to include the full set of nonlinear equations describing finite electron inertia, and the role played by finite electron inertia in the nonlinear dynamics of FLRs is currently under investigation.

In our simulations, the radial scale sizes for the resonances pose a very difficult problem for experimenters to verify. Satellite data might be used for these measurements, following the methods used by Singer et al. [1982]. It is not clear, though, that widths as narrow as $0.1 R_E$ could be accurately measured, bearing in mind temporal and spatial effects as the satellites traverse the resonances. It is also not clear that radar measurements in the E-region [Walker et al., 1979] or F-region [Walker et al., 1992] can attain the desired spatial resolutions, which should be smaller than approximately 5 km. One exciting possibility is in the use of optical measurements to determine the latitudinal widths of FLRs. Samson et al. [1991, 1992a] and Xu et al. [1993] have shown that FLRs can cause strong modulations in electron precipitation in the auroral ionosphere. However, their spatial resolution was too poor to determine much about the latitudinal structure of FLRs. If the electron precipitation is a direct result of the fields within the FLRs, perhaps due to the parallel fields associated with kinetic Alfvén waves or electron inertia waves, then ground-based optical

measurements of 5577Å and 6300Å emissions could easily be used to determine the structure of the FLRs.

Acknowledgments. This research was supported by the Natural Sciences and Engineering Research Council of Canada (NSERC). We would also like to thank J. P. DeVilliers and the staff of Myrias Computer Technologies of Edmonton, Alberta, Canada, for their help with the parallel implementation of the computer code on the Myrias SPS-3 parallel processor.

The Editor thanks M. Cao and another referee for their assistance in evaluating this paper

REFERENCES

- Allan, W., and E. M. Poulter, Damping of magnetospheric cavity modes: a discussion, *J. Geophys. Res.*, **94**, 11,843, 1989.
- Allan, W., S. P. White, and E. M. Poulter, Impulse-excited hydromagnetic cavity and field-line resonances in the magnetosphere, *Planet. Space Sci.*, **34**, 371, 1986.
- Goertz, C. K., Kinetic Alfvén waves on auroral field lines, *Planet. Space Sci.*, **32**, 1387, 1984.
- Harrold, B. G., and J. C. Samson, Standing ULF modes in the magnetosphere: a theory, *Geophys. Res. Lett.*, **19**, 1811, 1992.
- Hasegawa, A., Particle acceleration by MHD surface wave and formation of aurora, *J. Geophys. Res.*, **81**, 5083, 1976.
- Hughes, W. J., R. L. McPherron, and J. N. Barfield, Geomagnetic pulsations observed simultaneously on three geostationary satellites, *J. Geophys. Res.*, **83**, 1109, 1978.
- Inhester, B., Numerical modeling of hydromagnetic wave coupling in the magnetosphere, *J. Geophys. Res.*, **92**, 4751, 1987.
- Kivelson, M. G., and D. J. Southwood, Coupling of global magnetospheric MHD eigenmodes to field line resonances, *J. Geophys. Res.*, **91**, 4345, 1986.
- Lee, D.-H., and R. L. Lysak, Impulse excitation of ULF waves in a three dimensional dipole model, *J. Geophys. Res.*, **96**, 3479, 1991.
- Mitchell, D. G., M. J. Engebretson, D. J. Williams, C. A. Cattel, and R. Lundin, Pc 5 pulsations in the outer dawn magnetosphere seen by ISEE 1 and 2, *J. Geophys. Res.*, **95**, 967, 1990.
- Rankin, R., B. G. Harrold, J. C. Samson, and P. Frycz, The nonlinear evolution of field line resonances in the Earth's magnetosphere, *J. Geophys. Res.*, **98**, 5839, 1993.
- Samson, J.C., T.J. Hughes, F. Creutzberg, D.D. Wallis, R.A. Greenwald, and J.M. Ruohoniemi, Observations of a detached discrete arc in association with field line resonances, *J. Geophys. Res.*, **96**, 15,683, 1991.
- Samson, J. C., D. D. Wallis, T. J. Hughes, F. Creutzberg, J. M. Ruohoniemi, and R. A. Greenwald, Substorm intensifications and field line resonances in the nightside magnetosphere, *J. Geophys. Res.*, **97**, 8495, 1992a.
- Samson, J. C., B. G. Harrold, J. M. Ruohoniemi, R. A. Greenwald, and A. D. M. Walker, Field line resonances associated with MHD waveguides in the magnetosphere, *Geophys. Res. Lett.*, **19**, 441, 1992b.
- Seyler, C. E., A mathematical model of the structure and evolution of small scale discrete auroral arcs, *J. Geophys. Res.*, **95**, 17,199, 1990.
- Singer, H. J., W. J. Hughes, and C. T. Russell, Standing hydrodynamic waves observed by ISEE 1 and 2: radial extent and harmonic, *J. Geophys. Res.*, **87**, 3519, 1982.
- Walker, A. D. M., Modelling of Pc5 pulsation structure in the magnetosphere, *Planet. Space Sci.*, **28**, 213, 1980.
- Walker, A. D. M., The Kelvin-Helmholtz instability in the low-latitude boundary layer, *Planet. Space Sci.*, **29**, 1119, 1981.
- Walker, A. D. M., R. A. Greenwald, W. F. Stuart, and C. A. Green, STARE auroral radar observations of Pc5 geomagnetic pulsations, *J. Geophys. Res.*, **84**, 3373, 1979.
- Walker, A. D. M., J. M. Ruohoniemi, K. B. Baker, R. A. Greenwald, and J. C. Samson, Spatial and temporal behavior of ULF pulsations observed by the Goose Bay HF radar, *J. Geophys. Res.*, **97**, 12,187, 1992.
- Xu, B.-L., J. C. Samson, W. W. Liu, F. Creutzberg, and T. J. Hughes, Observations of optical aurora modulated by resonant Alfvén waves, *J. Geophys. Res.*, **98**, 11,531, 1993.

P. Frycz, R. Rankin, and J. C. Samson, Canadian Network for Space Research, University of Alberta, Edmonton, Alberta T6G 2E9, Canada.

(Received April 9, 1993;
revised July 15, 1993;
accepted July 20, 1993.)